CoA Report No. 129

THE COLLEGE OF AERONAUTICS

CRANFIELD

BASE PRESSURE AT SUBSONIC SPEEDS IN THE PRESENCE OF A SUPERSONIC JET

by

A. H. CRAVEN

REPORT NO. 129
March, 1960

THE COLLEGE OF AERONAUTICS

CRANFIELD

Base Pressure at Subsonic Speeds in the Presence of a Supersonic Jet

- by -

A. H. Craven, M.Sc., Ph.D., D.C.Ae.

SUMMARY

This paper presents the results of an experimental investigation into the effect of supersonic jets upon the base pressure of a bluff cylinder in a uniform subsonic flow. The ratio of jet diameter to base diameter was 0.1875.

Jet stagnation pressures giving slight under-expansion of the jet cause an increase in the base pressure but for larger jet stagnation pressures the base pressure is again reduced.

A simple theory, based on a momentum integral, shows the dependence of the base drag upon the jet and free stream speeds and upon the dimensions of the jet and the base.

The author wishes to acknowledge the permission given by the Commandant of the Royal Air Force Technical College to undertake at the College of Aeronautics, Cranfield, the study reported in this paper.

LIST OF CONTENTS

LIST OF SYMBOLS

C_{D_B}	base drag coefficient $\dfrac{\text{Base drag}}{\frac{1}{2}\rho_\infty u_\infty^2 \pi(R_B^2 - R_J^2)}$
C'_{D_B}	modified base drag coefficient defined in eqn. 15
C_J	jet momentum coefficient $mv_b/\frac{1}{2}\rho_\infty u_\infty^2 S$
C_{p_B}	base pressure coefficient
d	radius of mixing region in the plane of the velocity traverse
J	jet stagnation pressure parameter $\dfrac{P_J}{P_\infty} \dfrac{M_{J_D}}{\left(1+\frac{\gamma-1}{2}M_{J_D}^2\right)^{\frac{\gamma+1}{2(\gamma-1)}}}$
l	distance of the plane of the velocity traverse from the base
m	rate of jet mass flow
M_{J_D}	nozzle design Mach Number
P_J	jet stagnation pressure
p	static pressure
p_B	base pressure
p_J	jet static pressure at nozzle exit
r	radial distance from jet centre line
r′	radius of a vortex ring
$\bar{r}$	r/r'
R_B	base radius
R_J	jet radius
S	base area $\pi(R_B^2 - R_J^2)$
u	streamwise velocity
u_J	jet velocity at exit
v	velocity normal to free stream direction
v_b	equivalent jet velocity (jet velocity attained in isentropic expansion from jet stagnation pressure to free stream static pressure

List of Symbols (Continued)

x	distance downstream of base
x'	distance of vortex ring downstream of base
$\bar{x}$	x'/r'
ρ	density
ρ_J	jet density at nozzle exit
Γ	vortex strength
η	r/d
ξ	x/l

Suffices

∞	undisturbed free stream
1	free stream in plane of the base
2	free stream in plane of the velocity traverse
D	at nozzle design conditions

1. Introduction

In the past the majority of work on base pressures has concentrated upon the base in supersonic flow. A comprehensive bibliography has been prepared by Wilson (Ref. 1). Very little information is available on base drag in subsonic flow. The present author has considered the effect on the base drag of a subsonic jet in the choked and unchoked condition issuing from the base (Ref. 2). The effect of jet deflection (Ref. 3) and of body incidence (Ref. 4) have also been studied, both with a subsonic jet issuing from the base. In each case the base diameter has been large compared with the jet diameter.

It has been shown (Ref. 2) that, for a subsonic jet, the presence of a bubble (or a volume of recirculating fluid) extending from the base to some four body diameters downstream, and considerable regions of reversed flow, cause substantial reductions in the base pressure and increases in the base drag. These effects increase in magnitude as the jet stagnation pressure in increased.

The present paper presents the results of an experimental investigation into the effect of supersonic jets upon the base pressure on a bluff cylinder in uniform subsonic flow. The geometry of the base, jet diameter/ body diameter = 0.1875, is not intended to be representative of current aircraft practice, although it is fairly representative of the base geometry of unguided rockets. The main reason for selecting this geometry was a desire to explore the flow in the vicinity of the base and therefore the consequent advantages of using the above dimensions are obvious.

A simple theory, based on a momentum integral, is derived which shows the dependence of the base drag on the jet and free stream speeds and upon the dimensions of the jet and body. In order to confirm the flow pattern downstream of the base a simple potential flow model has been taken consisting of a toroidal vortex to represent the bubble and a line distribution of sinks along the jet centre-line to represent the entrainment effect of the jet. It is shown that this model yields a pressure distribution on the base similar to that obtained by experiment.

The author wishes to express his gratitude to Mr. G. M. Lilley for his help and encouragement throughout the study, to Dr. R. F. Sargent of the Bristol-Siddeley Aero-engine Company for providing the nozzle ordinates, to Mr. S. H. Lilley for the design and erection of the experimental equipment, to Mr. H. Stanton for making the nozzles and other equipment and to the laboratory assistants of the Aerodynamics Department who were largely responsible for taking the experimental measurements.

2. The dependence of the base drag coefficient on jet conditions

Consider the flow into and out of the element ABCDEF (Fig. 1). BC coincides with the base and EF is sufficiently far downstream for the element to include completely the bubble and any reversed flow.

Let the jet radius (AB) = R_J

the base radius (AC) = R_B

and the radius of the mixing region (FE) = d at a distance l downstream of the base.

We write δ to represent the boundary layer thickness on the body at C.

2.1. The basic equations

The equation of conservation of mass flow applied to the element yields

$$\int_{AB} 2\pi r\, \rho_J\, u_J\, dr + \int_{CD} 2\pi r\, \rho u\, dr = \int_{FE} 2\pi r\, \rho u\, dr + 2\pi d \int_{DE} \rho v\, dx \qquad \ldots\ldots \quad (1)$$

and from the conservation of momentum

$$\int_{AB} 2\pi r\, (p_J + \rho_J\, u_J^2)dr + \int_{BC} 2\pi r\, p_B\, dr + \int_{CD} 2\pi r\, (p_1 + \rho u^2)dr = \int_{FE} 2\pi r\, (p + \rho u^2)dr + 2\pi d \int_{DE} \rho v\, u\, dx \qquad \ldots\ldots \quad (2)$$

If we neglect the jet boundary layer thickness (1) can be written in the form

$$R_J^2\, \rho_J\, u_J + \left[d^2 - (R_B + \delta)^2\right] \rho_1 u_1 + 2\, \rho_1 u_1 \int_0^{\delta} (R_B + y) \frac{\rho u}{\rho_1 u_1}\, dy = 2\, d^2 \int_0^1 \rho u\, \eta\, d\eta + 2\, d\, l\, \rho_1 u_1 \int_0^1 \frac{\rho v}{\rho_1 u_1}\, d\xi \qquad \ldots\ldots \quad (3)$$

where $\eta = r/d$; $\xi = x/l$

and (2) becomes

$$R_J^2 (p_J + \rho_J u_J^2) + \left[d^2 - (R_B + \delta)^2 \right] (p_1 + \rho_1 u_1^2) + 2 \rho_1 u_1^2 \int_0^{\delta} (R_B + y) \frac{\rho u^2}{\rho_1 u_1^2} dy + 2 \int_{R_J}^{R_B} r\, p_B\, dr$$

$$= 2 d^2 \int_0^1 (p + \rho u^2)\, \eta\, d\eta + 2 dl\, \rho_1 u_1^2 \int_0^1 \frac{\rho v u}{\rho_1 u_1^2} d\xi \qquad (4)$$

2.2. The base drag

If now we define the base drag coefficient C_{D_B} by

$$C_{D_B} = \frac{2\pi \int_{R_J}^{R_B} (p_\infty - p_B)\, r\, dr}{\frac{1}{2} \rho_\infty u_\infty^2 \pi (R_B^2 - R_J^2)} \qquad (5)$$

which does not include the pressure integrated over the area of the jet at the nozzle exit, we can replace p_B in (4) from (5) to give

$$C_{D_B} \cdot \tfrac{1}{2} \rho_\infty u_\infty^2 (R_B^2 - R_J^2) = R_J^2 (p_J + \rho_J u_J^2) + p_\infty (R_B^2 - R_J^2)$$

$$+ \left[d^2 - (R_B + \delta)^2 \right] (p_1 + \rho_1 u_1^2) + 2 \rho_1 u_1^2 \int_0^{\delta} (R_B + y) \frac{\rho u^2}{\rho_1 u_1^2} dy$$

$$- 2 d^2 \int_0^1 (p + \rho u^2)\, \eta\, d\eta - 2 dl\, \rho_1 u_1^2 \int_0^1 \frac{\rho u v}{\rho_1 u_1^2} d\xi \qquad (6)$$

and, eliminating $R_J^2 \rho_J u_J$ between (3) and (6), we have

$$C_{D_B} \cdot \tfrac{1}{2} \rho_\infty u_\infty^2 (R_B^2 - R_J^2) = R_J^2 p_J + \left[d^2 - (R_B + \delta)^2 \right] (p_1 + \rho_1 u_1^2 - \rho \mu_1 u_J)$$

$$+ p_\infty (R_B^2 - R_J^2) + 2 \int_0^{\delta} (R_B + y)\, \rho u (u - u_J) dy$$

$$+ 2 d^2 \int_0^1 (\rho u u_J - \rho u^2 - p)\, \eta\, d\eta - 2 dl \int_0^1 \rho v (u - u_J) d\xi$$

..... (7)

Now with constant static pressure along FE

$$\int_0^1 p\,\eta\,d\eta = \frac{p_2}{2}$$

and (7) may be rewritten in the form

$$C_{D_B} = \frac{R_J^2\,(p_J - p_\infty)}{\frac{1}{2}\rho_\infty u_\infty^2 (R_B^2 - R_J^2)} + \frac{d^2(p_1 - p_2)}{\frac{1}{2}\rho_\infty u_\infty^2 (R_B^2 - R_J^2)} + \frac{R_B^2}{R_B^2 - R_J^2}\left[\frac{p_\infty - p_1(1 + \delta/R_B)^2}{\frac{1}{2}\rho_\infty u_\infty^2}\right]$$

$$+ 2\,\frac{\rho_1 u_1^2}{\rho_\infty u_\infty^2}\left(1 - \frac{u_J}{u_\infty}\right)\left(\frac{d^2 - (R_B + \delta)^2}{R_B^2 - R_J^2}\right) + \frac{4R_B^2}{R_B^2 - R_J^2}\int_0^{\delta}\left(1 + y/R_B\right)\left(\frac{u}{u_\infty} - \frac{u_J}{u_\infty}\right)\frac{\rho u}{\rho_\infty u_\infty}dy$$

$$+ \frac{4d^2}{R_B^2 - R_J^2}\int_0^1 \frac{\rho u}{\rho_\infty u_\infty}\left(\frac{u_J}{u_\infty} - \frac{u}{u_\infty}\right)\eta\,d\eta + \frac{4dl}{R_B^2 - R_J^2}\int_0^1 \frac{\rho v}{\rho_\infty u_\infty}\left(\frac{u_J}{u_\infty} - \frac{u}{u_\infty}\right)d\xi$$

..... (8)

It is reasonable to take the speeds u_1, u_∞ and the pressure p_1, p_2, p_∞ outside the mixing region equal respectively. Thus (8) reduces to

$$C_{D_B} = \frac{p_J - p_\infty}{\frac{1}{2}\rho_\infty u_\infty^2}\left(\frac{1}{R_B^2/R_J^2 - 1}\right) + 2\left(1 - \frac{u_J}{u_\infty}\right)\left(\frac{d^2 - R_B^2}{R_B^2 - R_J^2}\right)$$

$$+ \frac{4d^2}{R_B^2 - R_J^2}\cdot\frac{u_J}{u_\infty}\int_0^1 \frac{\rho u}{\rho_\infty u_\infty}\left(1 - \frac{u}{u_J}\right)\eta\,d\eta + \frac{4dl}{R_B^2 - R_J^2}\,\frac{u_J}{u_\infty}\int_0^1 \frac{v}{u_\infty}\left(1 - \frac{u}{u_J}\right)d\xi$$

..... (9)

where the boundary layer thickness δ has been assumed very small compared with R_B.

With the same approximations for the speeds and pressures outside the mixing region, equation (3) can be written

$$\frac{R_J^2 \rho_J u_J}{\left(R_B^2 - R_J^2\right) \rho_\infty u_\infty} + \frac{d^2 - R_B^2}{R_B^2 - R_J^2} = \frac{2 d^2}{R_B^2 - R_J^2} \int_0^1 \frac{\rho u}{\rho_\infty u_\infty} \eta \, d\eta + \frac{2 dl}{R_B^2 - R_J^2} \int_0^1 \frac{v}{u_\infty} \, d\xi$$

..... (10)

Now the last term of (9) is

$$\frac{4 dl}{R_B^2 - R_J^2} \int_0^1 \frac{v}{u_\infty} \left(\frac{u_J}{u_\infty} - \frac{u}{u_\infty} \right) d\xi$$

and along DE (which is outside the mixing region) $u = u_\infty$.

Thus

$$\frac{4 dl}{R_B^2 - R_J^2} \int_0^1 \frac{v}{u_\infty} \left(\frac{u_J}{u_\infty} - \frac{u}{u_\infty} \right) d\xi = \frac{4 dl}{R_B^2 - R_J^2} \left(\frac{u_J}{u_\infty} - 1 \right) \int_0^1 \frac{v}{u_\infty} \, d\xi \quad (11)$$

and, substituting from (10) and (11) into (9), we obtain

$$C_{D_B} = \frac{p_J - p_\infty}{\frac{1}{2} \rho_\infty u_\infty^2} \left(\frac{R_J^2}{R_B^2 - R_J^2} \right) + 2 \left(\frac{u_J}{u_\infty} - 1 \right) \frac{\rho_J u_J}{\rho_\infty u_\infty} \cdot \frac{R_J^2}{R_B^2 - R_J^2}$$

$$+ \frac{4 d^2}{R_B^2 - R_J^2} \int_0^1 \frac{\rho u}{\rho_\infty u_\infty} \left(1 - \frac{u}{u_\infty} \right) \eta \, d\eta \quad (12)$$

If we define a thrust coefficient C_T by

$$C_T = \frac{\text{Jet thrust}}{\frac{1}{2} \rho_\infty u_\infty^2 \pi (R_B^2 - R_J^2)}$$

then

$$C_T = \frac{p_J - p_\infty + \rho_J u_J^2}{\frac{1}{2} \rho_\infty u_\infty^2} \cdot \frac{R_J^2}{R_B^2 - R_J^2} \quad (13)$$

and (12) can be written

$$C_{D_B} = C_T + \frac{4\,d^2}{R_B^2 - R_J^2} \int_0^1 \frac{\rho\, u}{\rho_\infty\, u_\infty} \left(1 - \frac{u}{u_\infty}\right) \eta\, d\eta \qquad \ldots\ldots \quad (14)$$

for $u_J >> u_\infty$.

2.3. The case when $R_J << R_B$ and $u_J >> u_\infty$

If, in equation (12), we write

$$C'_{D_B} = C_{D_B} + \frac{p_\infty - p_J}{\frac{1}{2}\rho_\infty u_\infty^2} \left(\frac{R_J^2}{R_B^2 - R_J^2}\right) \qquad (15)$$

we have, since $d = R_B + \delta$ and δ is small compared with R_B,

$$C'_{D_B} = 4 \int_0^1 \eta \left[\frac{\rho_J\, u_J^2\, R_J^2}{\rho_\infty\, u_\infty^2\, R_B^2} \left(1 - \frac{u_\infty}{u_J}\right) - \frac{\rho\, u}{\rho_\infty u_\infty} \left(\frac{u}{u_\infty} - 1\right)\right] d\eta$$

Thus

$$u_\infty C'_{D_B} = \frac{4\,R_J^2}{R_B^2} \cdot \frac{\rho_{J_D}\, u_{J_D}}{\rho_\infty} \cdot \frac{\rho_J\, u_J}{\rho_{J_D}\, u_{J_D}^2} \int_0^1 \eta \left[\left(1 - \frac{u}{u_J}\right) \frac{u_{J_D}}{u_\infty} - \frac{R_B^2}{R_J^2} \frac{\rho u\, u_{J_D}}{\rho_J\, u_J^2} \left(\frac{u}{u_\infty} - 1\right)\right] d\eta \qquad (16)$$

where ρ_{J_D} and u_{J_D} are the density and velocity at the nozzle exit under design conditions.

Now

$$\frac{\rho_{J_D}\, u_{J_D}}{\rho_\infty} = \frac{P_{J_D}}{P_\infty} \sqrt{\frac{T_\infty}{\left(T_{J_D}\right)_{st}}} \cdot \sqrt{\gamma R\, T_\infty} \cdot \frac{M_{J_D}}{\left(1 + \frac{\gamma-1}{2} M_{J_D}^2\right)^{\frac{\gamma+1}{2(\gamma-1)}}} \qquad \ldots\ldots \quad (17)$$

and

$$\frac{\rho_J\, u_J^2}{\rho_{J_D}\, u_{J_D}^2} = \frac{P_J}{P_{J_D}} \qquad \ldots\ldots \quad (18)$$

when the exit velocity is supersonic for, then, $M_J = M_{J_D}$

Thus, provided the Mach number of the jet at exit is supersonic, we have by substituting (17) and (18) into (16)

$$u_\infty C'_{D_B} \sim \frac{P_J}{p_\infty} \cdot \frac{M_{J_D}}{\left(1+\frac{\gamma-1}{2} M_{J_D}^2\right)^{\frac{\gamma+1}{2(\gamma-1)}}} \int_0^1 \eta \left[\left(1 - \frac{u_\infty}{u_J}\right) \frac{u_{J_D}}{u_\infty} - \frac{R_B^2}{R_J^2} \frac{\rho u\, u_{J_D}}{\rho_J u_J^2} \left(\frac{u}{u_\infty} - 1\right) \right] d\eta \quad \ldots\ldots \quad (19)$$

From velocity traverses across the mixing region it has been found that for any particular jet and stream conditions the integrated second term in (19) is roughly independent of the position of the traverse (provided the position of the traverse is in the established wake) and that it is of the same order of magnitude as the first (constant) term. Thus we deduce that the integrand is nearly independent of u_J/u_∞ but is a function of the jet conditions u_J/u_{J_D} and ρ_J/ρ_{J_D}.

Hence

$$u_\infty C'_{D_B} = f\left[\frac{P_J}{p_\infty} \cdot \frac{M_{J_D}}{\left(1+\frac{\gamma-1}{2} M_{J_D}^2\right)^{\frac{\gamma+1}{2(\gamma-1)}}} \right] \quad (20)$$

Now the jet static pressure at exit is not markedly different from the free stream static pressure and $R_J \ll R_B$. Hence C'_{D_B} will be of the same order as C_{D_B}. Thus, defining a jet stagnation pressure parameter J by

$$J = \frac{P_J}{p_\infty} \cdot \frac{M_{J_D}}{\left(1+\frac{\gamma-1}{2} M_{J_D}^2\right)^{\frac{\gamma+1}{2(\gamma-1)}}}, \quad (21)$$

we have for large jet velocities

$$u_\infty C_{D_B} = f(J) \quad (22)$$

It is shown in Fig. 3 that the results for the base drag coefficients, found in the experiments described in later sections of this paper, for different jet design Mach numbers collapse on the basis of $u_\infty C_{D_B}$ plotted against J for supersonic exit velocities.

2.4. The case when $R_J \ll R_B$ and $u_J < u_\infty$

Although accurate experimental results are not available for the case when the jet velocity is less than the free stream speed, it is of interest to consider the case for it represents the problem of "base bleed" associated with a small central jet.

From equations 12 and 13 if $d = R_B$, $R_B \gg R_J$ and

$$\frac{u_J}{u_\infty} < 1$$

$$C_{D_B} - C_T = - \frac{2 \rho_J u_J}{\rho_\infty u_\infty} \frac{R_J^2}{R_B^2} + 4 \int_0^1 \frac{\rho u}{\rho_\infty u_\infty} \left(1 - \frac{u}{u_\infty}\right) \eta \, d\eta$$

If $C_T \approx 0$ it is seen that, because the integral is always positive, the base drag is reduced when $\rho_J u_J > 0$ and $u_J < u_\infty$

3. Apparatus

3.1. The wind tunnel and instrumentation

The tests were performed in a straight through wind tunnel having a closed working section measuring 3 ft. square. The compressed air supply for the jet was led along the centre line of the tunnel to the working section in a $3\frac{1}{2}$ in. diameter pipe which was threaded at its downstream end to attach the models. The supply pipe was encased in a duralumin sleeve 4 in. in diameter, the space between the sleeve and the supply pipe being occupied by the pressure tubes. The surface pressures from the model were read from a multi-tube water manometer.

3.2. The models

The models used in these tests were each right cylinders 4 in. in diameter and 12 in. long turned from light alloy. The internal cavity of each model was machined to give smooth internal flow into a convergent-divergent nozzle $\frac{3}{4}$ in. exit diameter, each model having a nozzle designed to give parallel flow at the jet exit at its design Mach number. The design Mach numbers of the nozzles, allowing for a nominal boundary layer correction, were 1.0, 1.2, 1.4, 1.6, 1.8 and 2.0. An internal gauze screen was fitted between the model and the supply pipe to eliminate non-uniformities in the compressed air flow from the supply pipe into the model's pressure cavity.

Polythene tubing for pressure measurements was inserted in slots along the base radii and the models generators at angular intervals of $22\frac{1}{2}^\circ$ and secured with araldite.

4. The Scope of the Tests

The tests on each of the models covered a range of free stream speeds from 50 to 100 ft/sec. The actual "design" Mach numbers M_{J_D} of the nozzles tested were 1.0, 1.23, 1.41, 1.60, 1.82 and 1.98. Defining the jet stagnation pressure parameter J as in equation 21, i.e.

$$J = \frac{P_J}{p_\infty} \cdot \frac{M_{J_D}}{\left(1 + \frac{\gamma - 1}{2} M_{J_D}^2\right)^{\frac{\gamma+1}{2(\gamma-1)}}}$$

where P_J = jet stagnation pressure

p_∞ = free stream static pressure

M_{J_D} = jet design Mach number,

sufficient jet stagnation pressure was available to enable J to be varied in the range 0 to 4.0.

The thickness of the turbulent boundary layer on the side of the body at the base section is 0.6" approximately from which we deduce that the effective length of the body is 2.3 ft. Based on this length and a tunnel speed of 100 ft/sec., the Reynolds number of these tests was 1.5×10^6.

5. Test procedure

The ordinary pressure plotting techniques were used in these tests. Pressure measurements were taken at tunnel speeds of 50, 55, 60, 65, 70, 80, 90, 100 and 120 ft/sec. for each of twelve jet stagnation pressures.

Total head and static pressure traverses were made in a diametral plane across the jet and mixing region at two, three, four, six and eight body diameters downstream of the base. The total head measurements were made using a Conrad yawmeter from which the flow direction at any station was determined. The static tube was aligned in this direction when making static pressure measurements. The total head and static tubes were calibrated at low speeds; no further corrections being applied to the readings.

6. Results

6.1. Presentation of results

The analysis of section 2 shows that the product of base drag coefficient and free stream speed is dependent only on jet conditions for the supersonic jet. We may infer that the product of the base pressure coefficient and free stream speed also depends only on jet conditions and is independent of free stream speed. Thus the pressure distribution on the base is presented in the form of graphs of $C_p u_\infty$ against r/R for given values of the jet stagnation parameter J (Figs. 2 b - d).

The base pressures have been integrated over the base to determine the base drag coefficient C_{D_B} referred to base area $[\text{i.e. } \pi(R_B^2 - R_J^2)]$ and free stream speed. $C_{D_B} u_\infty$ is plotted against jet stagnation pressure J in Fig. 3.

The foregoing method of presentation breaks down for low values of jet stagnation pressure. It is known (Ref. 2) that the base pressure and base drag coefficients in subsonic flow with no jet are constant and independent of free stream speed. It is to be expected that any $C_{D_B} u_\infty$ curve would break up into several branches (one for each tunnel speed) for values of J less than J_D. However for such jet stagnation pressures it is known that the flow from any of the nozzles is subsonic and it has been shown (Ref. 2) that, for subsonic jet flow, the base pressure and base drag coefficients are properly presented in terms of the jet momentum coefficient C_J defined by

$$C_J = \frac{m\, v_b}{\frac{1}{2}\, \rho_\infty u_\infty^2\, S}$$

where m is the rate of mass flow from the jet and v_b is the equivalent jet velocity (i.e. the velocity which the jet would attain in isentropic expansion from its stagnation pressure to free stream static pressure.

Figs. 5 a - f show clearly this dependence and the point at which this presentation also breaks down. The radial pressure distribution for the subsonic jet is shown in Fig. 2a in terms of C_J.

6.2. The base pressure distribution (Fig. 2)

For any given jet conditions the base pressure distribution follows the same general pattern. From the edge of the jet the base pressure falls with increase of radial position to a minimum at 0.7 R_B approximately, after which it rises steadily to the circumference of the base. The position of the minimum base pressure moves outwards from 0.68 R_B at the low values of jet stagnation pressure to 0.73 R_B at the highest available pressures. A variation from the general pattern of the pressure distribution was noticed near the jet exit for values of J less than J_D. In the region from the jet exit ($r/R_B = 0.1875$) to some point close to $r/R_B = 0.3$ the base pressure rises slightly before conforming to the general reduction noted previously. Furthermore the position of maximum base pressure moves inwards as the jet stagnation pressure is increased up to J_D. When the nozzle is at its design condition the pressure variation in the region $0.1875 < r/R_B < 0.3$ is negligible.

At any radial position the base pressure falls as the jet stagnation pressure rises to its design value for any nozzle. As P_J increases further in the range $J_D \leq J \leq 3.0$ the base pressure rises only to fall again for $J > 3.0$.

6.3. The base drag (Fig. 3)

The base drag coefficient increases with jet stagnation pressure for J less than J_D. For J between J_D and 3.0 increase of jet stagnation pressure causes a substantial reduction of base drag coefficient; but for J greater than 3.0 the base drag coefficient again increases.

6.4. The velocity distribution in the mixing region

Reliable velocity traverses were obtainable only at distances greater than four body diameters downstream of the base. In all cases the velocity distribution was of the form shown in Fig. 1. The distributions, when integrated according to equations 12 and 16 of paragraph 2, gave values of the base drag coefficient shown in Fig. 4.

Examples of the velocity distributions are given in Figs. 11 and 12. The readings from which these distributions were obtained were taken in regions where the jet flow had become subsonic.

7. Discussion

7.1. Accuracy of the results

The jet stagnation pressure was maintained, by continual adjustment of the control valve, to an accuracy better than 2.5% during any test. The tunnel speed could be kept constant to within 1% and the surface pressures measured to an accuracy of 0.02 in. of water. Hence the overall error in the pressure coefficients and in the base drag coefficients is considered to be less than 5%. This is borne out by examination of Fig. 3 in which maximum and minimum values are shown.

No account has been taken of tunnel interference effects. Any errors from this cause are expected to be small since the jet was aligned along the tunnel centre-line and the tunnel speed was adjusted to its prescribed value as the jet stagnation pressure was altered and before any pressure readings were taken.

7.2. The flow in the base region

The flow in the base region, for zero jet velocity, consists of a large volume of slowly recirculating flow (bubble or, if idealised, a toroidal vortex). Only at some three to four body diameters downstream of the base (Fig. 6a) is the wake well established. The form of the base pressure distributions and the regions of very slow and reversed flow indicated by the velocity traverses show that, in the presence of a jet, the bubble still exists and from its inside edge flow is entrained into the jet.

When the jet stagnation pressure is less than the nozzle's design pressure the jet flow is subsonic everywhere in the nozzle or passes through a normal shock in the divergent portion and is subsonic at exit. For the subsonic jet the maximum base pressure occurs near $r/R_B = 0.3$ (Fig. 2a) and indicates the existence of an attachment line there. The air impinging upon this line comes from the boundary layer on the body (Fig. 6b) and thus has a stagnation pressure much less than that of the free stream. The falling pressure gradient inwards is indicative of flow towards the jet along the inner portion of the base radii for the low jet speed (Fig. 6b). As the jet velocity is increased the bubble decreases in length and consequently the base pressure becomes more negative. Entrainment into the jet increases with increase of the jet velocity. In other words the vortex gets stronger with increase in jet velocity. It is also noted (Fig. 2a) that the attachment line moves inwards towards the edge of the jet as the jet speed increases.

These trends continue until the jet reaches sonic velocity (for the convergent nozzle) or its design Mach number (for convergent-divergent nozzles). For this condition the bubble is shortest and the attachment line has moved to the edge of the jet (Fig. 6c). The flow on the inner portions of the base is outwards and very slow.

In a slightly under-expanded jet (i.e. the jet stagnation pressure slightly greater than the design value) the length of the pseudo-laminar mixing region originating at the jet exit is greater than that for a jet at its design condition. This means that the strong extrainment occurs at some distance from the base (Fig. 6d). Hence the length of the bubble must increase causing the base pressure to increase (i.e. C_{D_B} is reduced slightly).

For a more highly under-expanded jet the extra expansion of the jet as it leaves the nozzle results in a smaller bubble (Fig. 6e). The vortex strength must increase causing the base pressure to be more negative. For large under-expansions the jet displacement effect tends to fill up the region downstream of the base and for still larger jet stagnation pressures, the jet gives a compressive effect on the external flow (Fig. 6f). Thus it is conjectured that the base pressure reaches a maximum suction for certain jet conditions and then must increase with further increase of jet stagnation pressure. This second maximum in, and subsequent reduction of, base suction was outside the range of jet stagnation pressure available in the experiment.

The structure of the axi-symmetric recirculating flow postulated here has similar properties to those of the two-dimensional laminar separation bubble described by Burrows and Newman (Ref. 5).

7.3. The base pressure and the base drag.

Previously (Ref. 2) it has been shown that, for subsonic jets, the base pressure distribution and the base drag coefficient are independent of free stream speed when plotted against the jet momentum coefficient C_J defined by

$$C_J = \frac{m\, v_b}{\frac{1}{2}\rho\, U_\infty^2\, S}$$

variations with forward speed only being apparent for jet stagnation pressures approaching that at which the nozzles choked. For a supersonic nozzle, C_J is again the controlling parameter provided that the jet stagnation pressure is not sufficiently large to choke the nozzle (Fig. 5). As the nozzle design pressure is approached variations with forward speed are again apparent but, for jet stagnation pressures exceeding twice the design pressure, the dependence of base drag coefficient on jet momentum coefficient is not affected by free stream speed. Comparison of Figs. 5a - f show that the presentation of C_D against C_J still leaves a dependence upon the nozzle design Mach number.

The theory of paragraph 2 shows that, for a base diameter considerably larger than the jet diameter, the product of the base drag coefficient and free stream speed is dependent only upon conditions in the jet. As base drag is obtained by integration of the base pressure, we would expect from the theory that the product of base pressure and free stream speed is also dependent only upon jet conditions.

For jet stagnation pressures approaching and exceeding the design pressure it is shown in Fig. 2 that, whatever nozzle was used, the product $c_p u_\infty$ is dependent only upon the jet stagnation pressure parameter J and not explicitly upon the jet stagnation pressure or the design Mach number of the nozzle. In Fig. 3 the dependence of $C_{D_B} u_\infty$ upon J is shown. In this figure the maximum and minimum values for $C_{D_B} u_\infty$ are shown for the different nozzles at various values of J and it is clear that the resulting curve is independent of the jet Mach number explicitly provided the jet stagnation pressure is greater than the design value.

The subsonic base drag for a base without jet is a constant independent of free stream speed. It is therefore not surprising that there is considerable scatter in the values of $C_{D_B} u_\infty$ for J less than J_D. The departure of the experimental results from the theoretical prediction for low jet stagnation pressures is attributed to imperfect establishment of the entrained flow downstream of the base for such jet conditions.

For values of J greater than J_D the jet is under-expanded and, as it leaves the nozzle considerable expansion occurs. Further the mixing region near the jet exit is probably pseudo-laminar and significant entrainment occurs only downstream of the compression region in the jet. The effect of this expansion on the base pressure has been discussed in the previous section. It is summarised in Fig. 7.

7.4. Comparison between theory and experiment (Fig. 4)

The base drag calculated from the velocity traverses and equation 12 of section 2, shows reasonable agreement with that obtained by direct integration of the base pressure distribution for the same jet conditions. The theory can be simplified in the case when $R_J \ll R_B$ and $u_J \gg u_\infty$ giving a value of base drag which underestimates the experimental value only slightly. The general expression tends to overestimate the base drag by some five per cent.

7.5. A potential flow model to represent the mixing region

In an attempt to show that the flow in the mixing region postulated in previous reactions is consistent with the experimental results a simple potential flow model has been considered. The model, which is described more completely in the appendix to this paper, represents only the flow outside the jet itself. The recirculating flow is represented by a vortex ring of strength Γ and radius r' at a distance x' downstream of the base. The entrainment effect of the jet is represented by a distribution of sinks along the jet centre line. By setting up the appropriate image system the base automatically becomes a streamline, and the radial velocity on the base can be calculated.

The pressure distributions calculated from the radial velocity show the same general trends as the experimental distributions but there are some wide differences in the magntiudes of the pressure coefficients involved. The major source of error lies in the use of free stream static pressure and speed as reference conditions. Since the recirculating and entrained flows near the base come mainly from the boundary layer of the body it is necessary to use as reference conditions some lower value of speed as a reference. In the appendix a speed equal to the average speed in the boundary layer was used with some improvement to the correlation between experimental and theoretical values (Figs. 9 and 10).

The model fails in that it is necessary to use experimentally determined boundary conditions to determine the values of the vortex strength and position. A much more sophisticated model is necessary if one wishes to predict base pressures by purely theoretical means. The model postulated here does not make the radial velocity zero at the outer edge of the base. Even so the pressure predicted there is not seriously in error and the movement of the centre of the recirculating flow and its increase in velocity is also predicted to a certain extent. The results obtained from this model are sufficient to show that the actual flow in the base region is as described in previous sections of this paper.

8. Conclusions

1. When the supersonic nozzle is not choked, the base pressure falls (and base drag increases) with increase of jet stagnation pressure.

2. For choked nozzles (designed for Mach numbers in the range from 1 to 2) an increase of jet stagnation pressure beyond the design pressure ($J_D < J < 3.0$) causes an increase in base pressure. Further increase of jet stagnation pressure ($J > 3.0$) again causes a reduction in base pressure.

3. The flow downstream of a large base consists of a toroidal bubble covering most of the base area. The flow entrained into the jet near the nozzle exit comes from the edge of this recirculating region. The normal flow associated with jet mixing is established only some three to four body diameter downstream of the base. The size of the bubble is reduced with increase of jet stagnation pressure.

4. A simple momentum analysis and an elementary potential flow model give results consistent with the postulated flow in the mixing region.

9. References

1. Wilson, C.W.J. — Base Pressure and Jet Effects on Afterbody Base and Adjacent Surfaces. R.A.E. Library Bibliography 196, February 1958.

2. Craven, A.H. — Interference of a rearward facing jet on the flow over three representative afterbody shapes. College of Aeronautics Note No. 60, April 1957.

3. Craven, A.H. — The effect of jet deflection on the interference of a rearward facing jet. College of Aeronautics Note No. 70, October 1957.

4. Craven, A.H. — Effect of body incidence on two afterbodies with a rearward facing jet. College of Aeronautics Note No.92, December 1958.

5. Burrows, F.M., Newman, B.G. — The application of suction to a two-dimensional laminar separation bubble. Mississippi State University Department of Aerophysics Research Report 27, October 1959.

6. Craven, A.H. — The effect of density on jet flow at subsonic speeds. College of Aeronautics Report No.120, July 1959.

A potential flow model for the flow in the vicinity of a bluff base

In order to establish the effect, on the base pressure distribution, of the viscous and turbulent mixing processes in the separated flow region downstream of the base it is instructive to consider the corresponding potential flow model. Only the region outside the jet will be considered. The inflow into the jet is represented by a continuous distribution of sinks of strength q per unit length on the axis of the jet. The circulating flow in the base region is represented by a vortex ring of strength Γ and radius r' placed at x' downstream of the base (Fig. 8). To satisfy the condition of no flow normal to the base an image vortex ring of strength $-\Gamma$ is taken at $-x'$ and a continuous distribution of sinks is placed on the reflection of the jet centre line. The external flow is represented by a surface distribution of sources of strength $\rho_\infty u_\infty \, r \, d\theta$ per unit length in the plane $x = 0$ and in the region $R_B \leq r \leq \infty$. This source distribution is assumed to give no flow radially in the plane $x = 0$. It should be noted that this model only attempts to represent the flow on and downstream of the base.

By virtue of the radial symmetry, the radial flow along the base $x = 0$ is given by

$$v(r) = \frac{x' \, r' \, \Gamma}{2\pi} \int_0^{2\pi} \frac{\cos\theta \, d\theta}{\left[x'^2 + r^2 + r'^2 - 2 \, r \, r' \cos\theta\right]^{3/2}} - \frac{1}{2\pi} \int_0^{\infty} \frac{q \, r \, dx}{(x^2 + r^2)^{3/2}}$$

$$= \frac{\Gamma \, x'/r'}{\pi r' \sqrt{\left(\frac{x'}{r'}\right)^2 + \left(1 + \frac{r}{r'}\right)^2}} \left[K(k) - \left(1 + \frac{2r/r'}{(x'/r')^2 + (\frac{r}{r'} - 1)^2} \right) E(k) \right] - \frac{q}{2\pi r} \qquad \ldots\ldots \quad (A.1)$$

where $K(k)$, $E(k)$ are respectively complete elliptic integrals of the first and second kind

$$k = \frac{4 \, r/r'}{(x'/r')^2 + (1 + r/r')^2}$$

and q has been taken constant,

or writing $x'/r' = \bar{x}$ and $r/r' = \bar{r}$

$$v(r) = \frac{\Gamma}{\pi r'} \cdot \frac{\bar{x}}{\left[\bar{x}^2+(1+\bar{r})^2\right]^{\frac{1}{2}}} \left[K(k) - \left\{ 1 + \frac{2\bar{r}}{\bar{x}^2+(\bar{r}-1)^2} \right\} E(k) \right] - \frac{q}{2\pi r} \quad \ldots\ldots \quad (A.2)$$

where $k = \dfrac{4\bar{r}}{\bar{x}^2+(1+\bar{r})^2}$

It is now necessary to determine values for the vortex strength Γ and its position $(\bar{x}, r')$ from boundary conditions. We note that the base pressure is a minimum at $r/R_B = 0.7$ approximately from which we deduce that the radius r' of the vortex ring is given by $r'/R_B = 0.7$.

Case 1. The subsonic jet

From the experimental results it can be seen that $v = 0$ when $r/R_B = 0.3$; i.e. $\bar{r} = 0.417\ R_B$. Thus (A.2) becomes

$$\frac{\Gamma \bar{x}}{1.558\left[\bar{x}^2+2.008\right]^{\frac{1}{2}}} \left[K(k) - \left\{ 1 + \frac{0.834}{\bar{x}^2+0.340} \right\} E(k) \right] - \frac{q}{1.882} = 0 \quad \ldots\ldots \quad (A.3)$$

with $k = \dfrac{1.668}{\bar{x}^2 + 2.008}$

The pressure coefficient based on free stream conditions and measured at $r = r'$ shows that

$$\frac{v(r')}{u_\infty} = 1.25$$

for $u_J/u_\infty = 6$

and (A.2) becomes

$$\frac{\Gamma \bar{x}}{\left[\bar{x}^2 + 4\right]^{\frac{1}{2}}} \left[K(k) - \left\{ 1 + \frac{2}{\bar{x}^2} \right\} E(k) \right] - \frac{q}{2} = 2.744\ u_\infty R_B \quad (A.4)$$

with $k = \dfrac{4}{\bar{x}^2 + 4}$

We may approximate to the strength of the sink distribution representing the jet by applying the results of Ref. 6. For $u_J/u_\infty = 6$ we find

$$q \approx \frac{m_J}{20\ \rho_\infty R_J}$$

where m_J $(=\pi \rho_J\ u_J\ R_J^2)$ is the mass flow in the jet

$$\text{i.e.} \qquad q \approx \frac{\pi}{20}\ u_J\ R_J \qquad \text{(A.5)}$$

Substituting from (A.5) into (A.4) and (A.3) and solving we find

$$\begin{aligned} \bar{x} &= 3.10 \\ \Gamma &= 44.4 \end{aligned} \qquad \text{(A.6)}$$

and thus, for a subsonic jet ($u_J/u_\infty = 6$), the radial velocity distribution (A.2) may be written

$$\frac{v(r)}{u_\infty} = \frac{62.6/R_B}{\left[9.60 + (1 + \bar{r})^2\right]^{\frac{1}{2}}} \left[K(k) - \left\{1 + \frac{2\bar{r}}{9.60 + (\bar{r} - 1)^2}\right\} E(k)\right] - \frac{0.025\ R_B}{r} \qquad \text{(A.7)}$$

and $$k = \frac{4\bar{r}}{9.60 + (1 + \bar{r})^2}$$

On the assumption that the pressure at the point $r/R_B = 0.3$ where $v = 0$ is the stagnation pressure of the free stream, the radial pressure distribution has been calculated for the case $u_J/u_\infty = 6$ and is shown as curve A-A in Fig. 9 and compared with an experimentally determined pressure distribution C-C. The main discrepancy lies near the attachment point where we have assumed that full free stream stagnation pressure is reached. However the flow attaching at $r/R_B = 0.3$ comes from the boundary layer on the body and is thus at a much lower total pressure than free stream. If now we take the average speed in the boundary layer at the end of the body as the reference speed and the static pressure as measured at the end of the body as a reference pressure and calculate the radial pressure distribution we obtain the curve shown as B-B in Fig. 9.

Case 2. The Sonic Jet

In this case the attachment point has moved to the edge of the jet and we may take $u_J/u_\infty = 10$. From Ref. 6 it is seen that the appropriate sink strength is given by

$$q \approx \frac{\pi u_J R_J}{10}$$

With the boundary conditions

(i) $v = 0$ when $r/R_B = 0.1875$

(ii) $C_p = 1.0$ (i.e. $\frac{v}{u_\infty} = 1.4$) when $r/R_B = 0.70$

we find that (A.2) yields

$$\bar{x} = 2.86$$

$$\Gamma = 48.6$$

Substitution of these values in (A.2) allows the radial pressure distribution to be calculated as before. Comparison of the theoretical and experimentally determined pressure distributions are given in Fig. 10

Case 3. The supersonic jet

The experimental results suggest that the attachment point does not move once the jet has become supersonic. Thus the only variations in Γ and $\bar{x}$ come from variations in the sink strength q which is dependent upon the speed ratio u_J/u_∞. However we may infer from Ref. 6 that an increase in u_J/u_∞ above 10 has little effect on q and hence we may deduce that the radial pressure distribution which the potential flow model predicts for the supersonic jet will vary little from that found for the sonic jet.

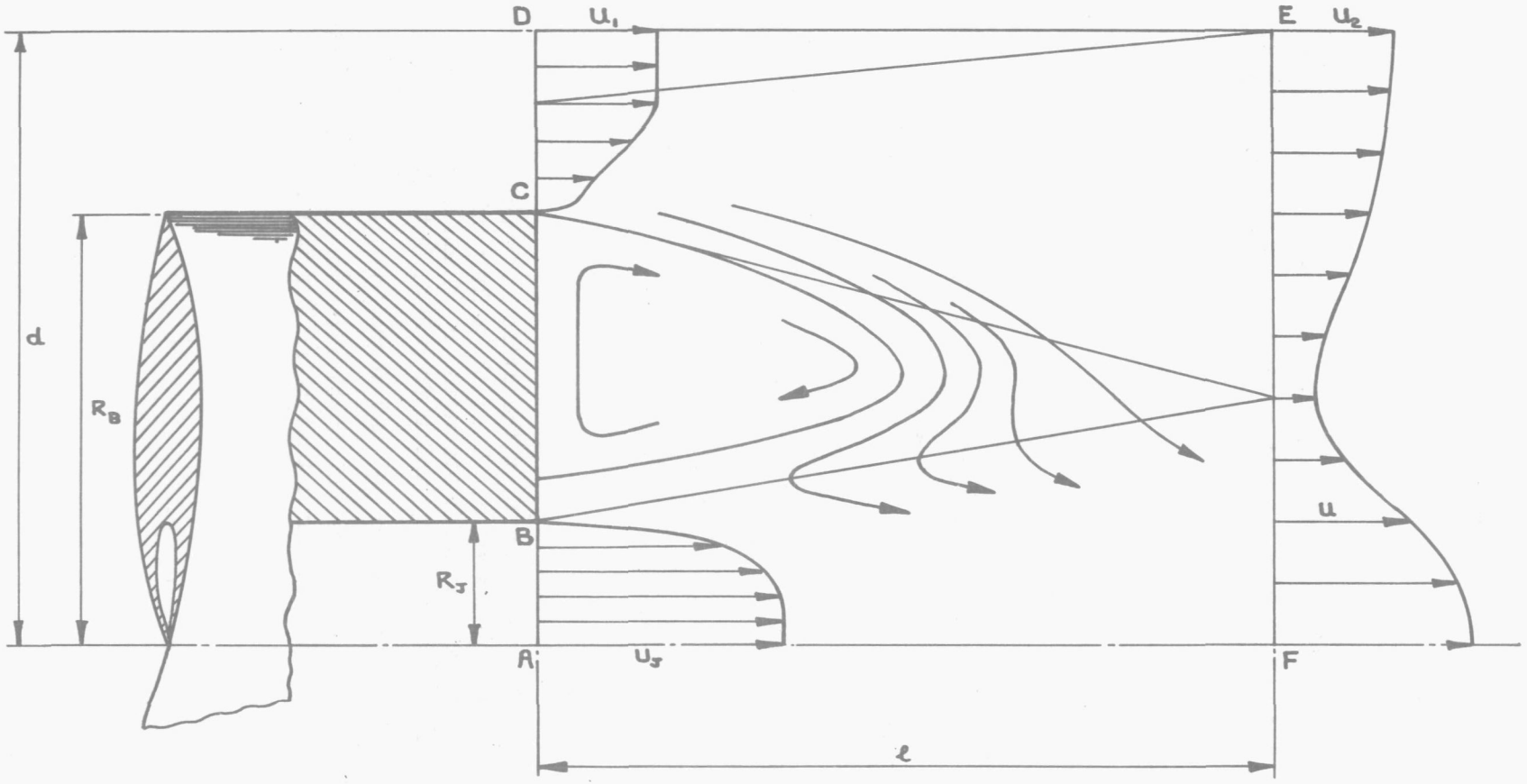

FIG. I. THE REGION CONSIDERED IN THE MOMENTUM INTEGRAL.

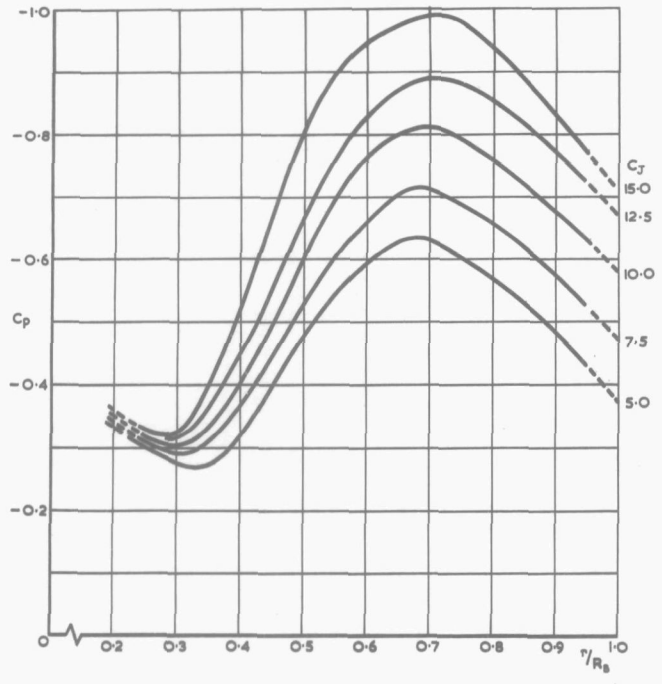

FIG. 2a. JET SUBSONIC.

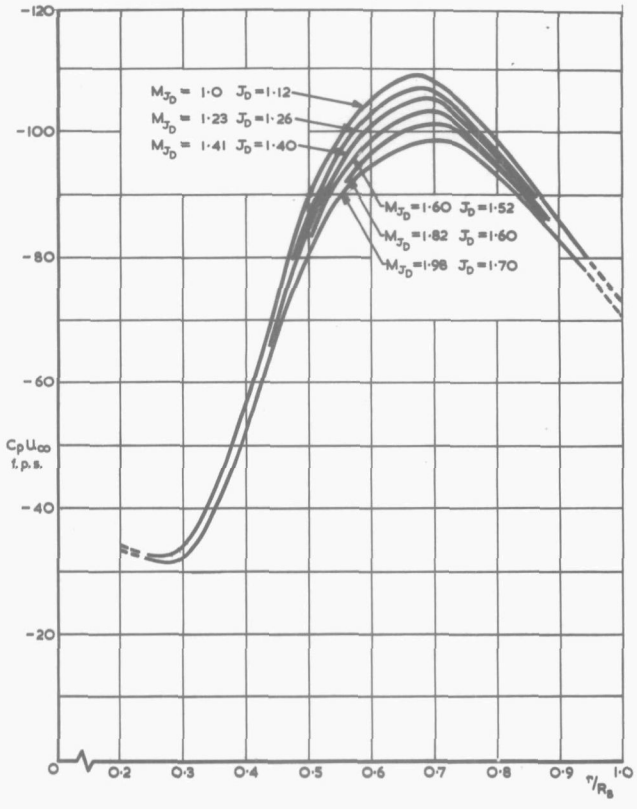

FIG. 2b. JET AT DESIGN CONDITIONS.

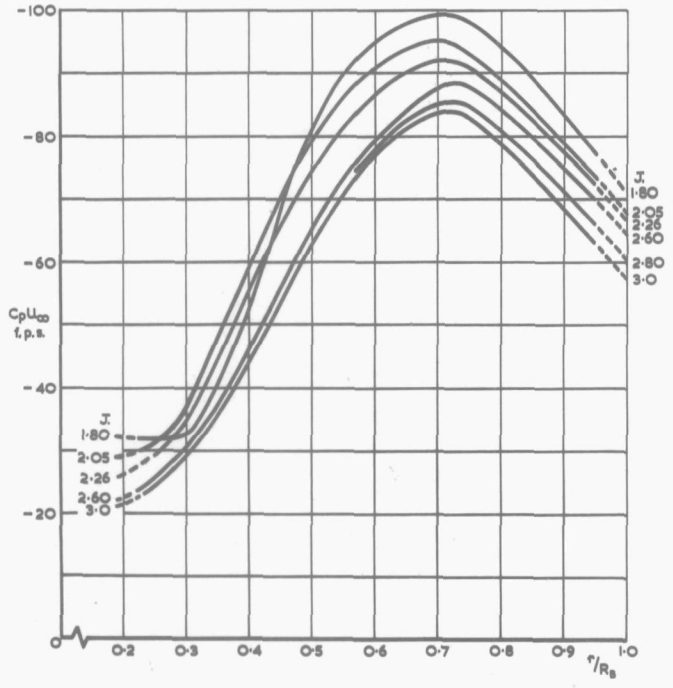

FIG. 2c. JET UNDER-EXPANDED $J_D < J \leq 3{\cdot}0$

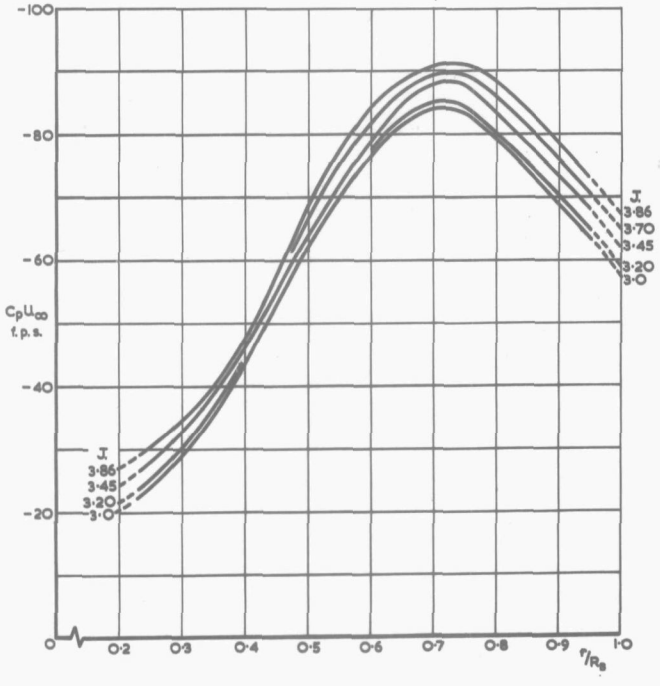

FIG. 2d. JET UNDER-EXPANDED $J > 3{\cdot}0$

FIG. 2. RADIAL PRESSURE DISTRIBUTIONS.

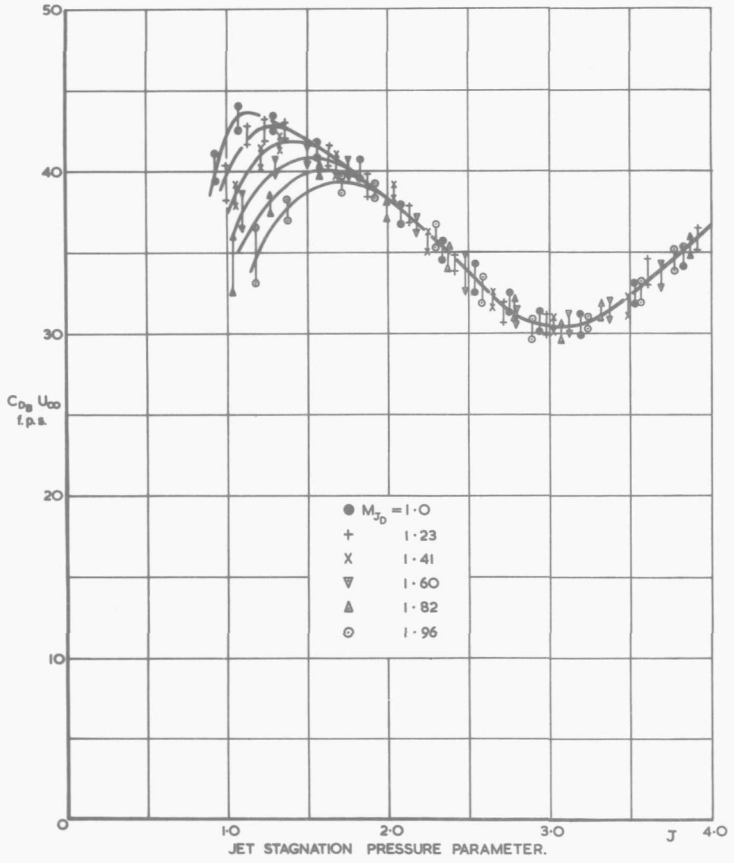

FIG. 3. VARIATION OF BASE DRAG COEFFICIENT WITH JET STAGNATION PRESSURE AND NOZZLE DESIGN MACH NUMBER.

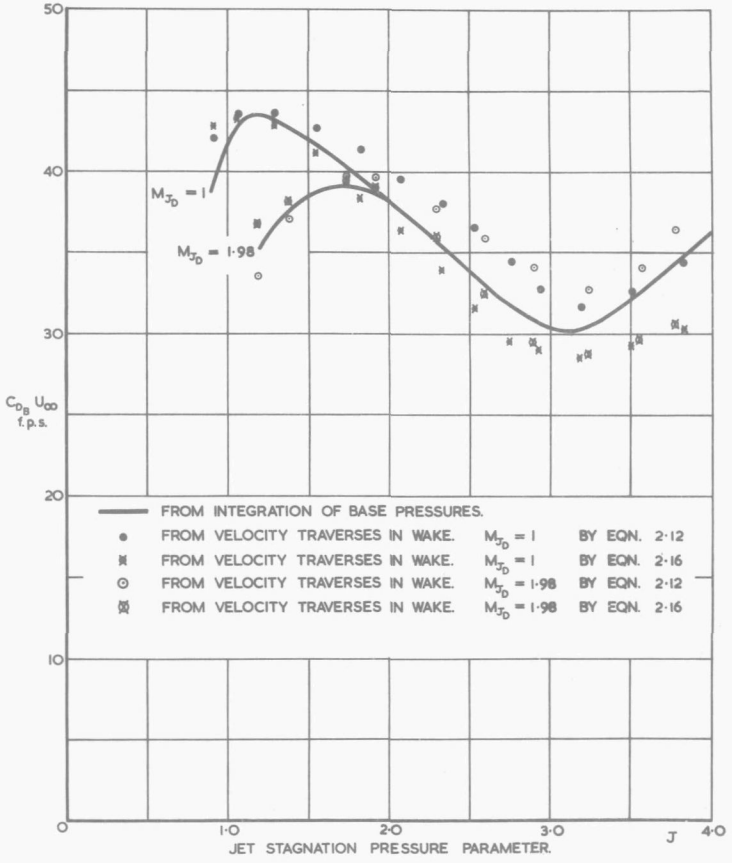

FIG. 4. COMPARISON OF BASE DRAG COEFFICIENTS OBTAINED FROM THE BASE PRESSURES AND FROM VELOCITY TRAVERSES.

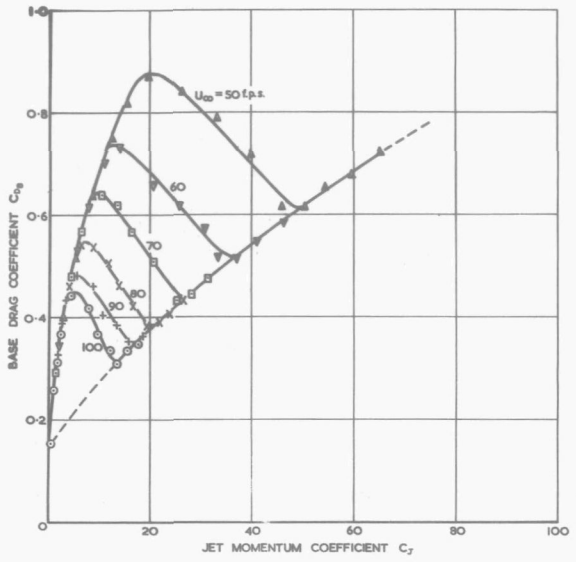

FIG. 5a. SONIC JET.

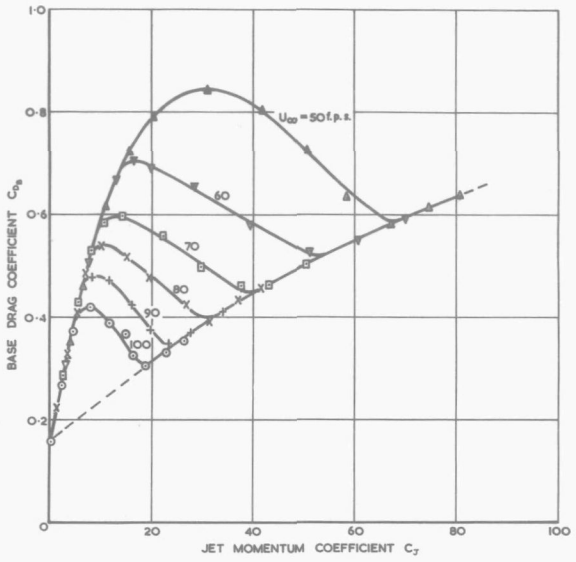

FIG. 5b. $M_{J_D} = 1 \cdot 23$

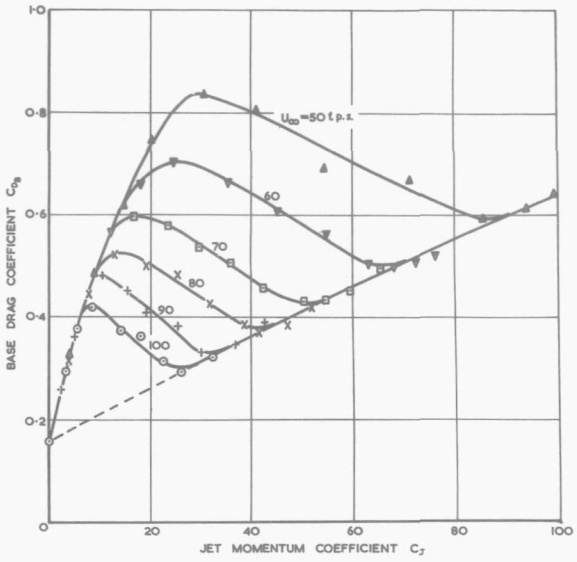

FIG. 5c. $M_{J_D} = 1 \cdot 41$

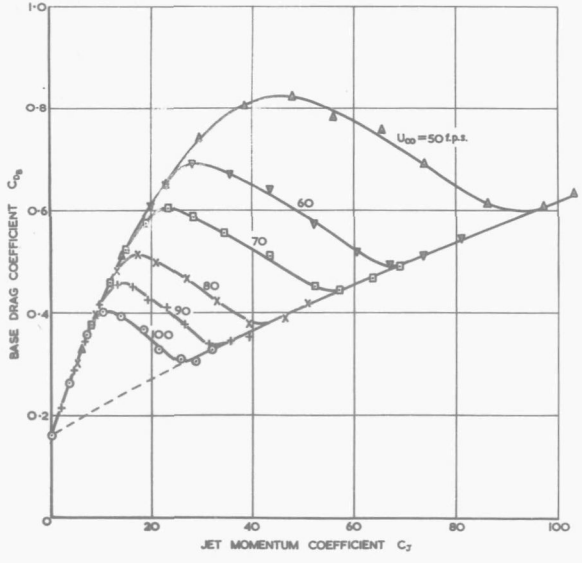

FIG. 5d. $M_{J_D} = 1 \cdot 60$

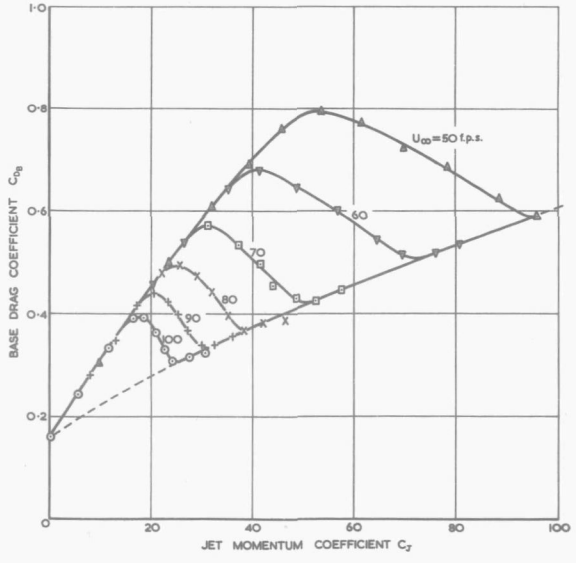

FIG. 5e. $M_{J_D} = 1 \cdot 82$

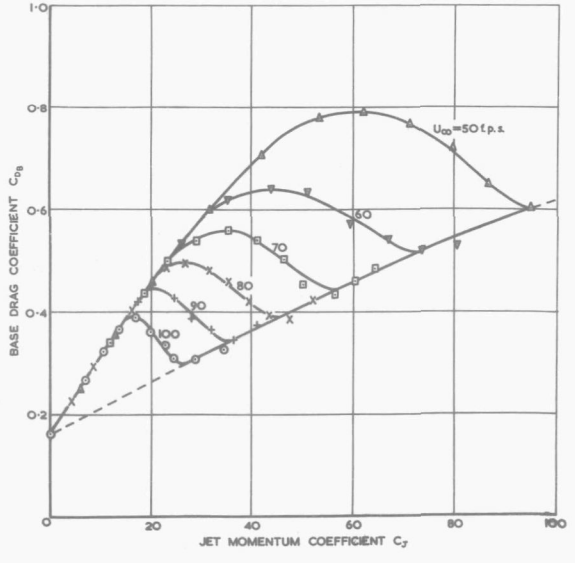

FIG. 5f. $M_{J_D} = 1 \cdot 98$

FIG. 5. VARIATION OF BASE DRAG COEFFICIENT WITH JET MOMENTUM COEFFICIENT.

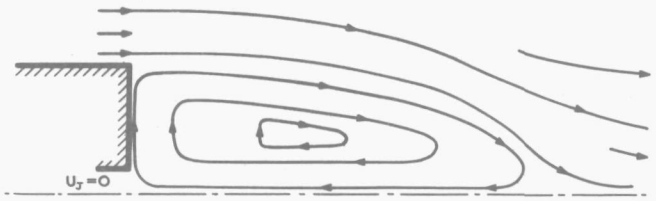

FIG. 6a. NO JET.

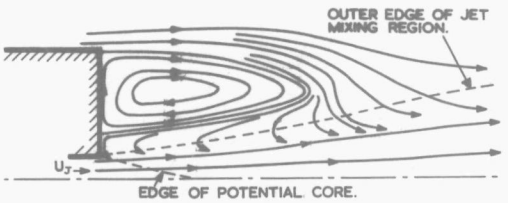

FIG. 6b. JET VELOCITY SMALL AND SUBSONIC.

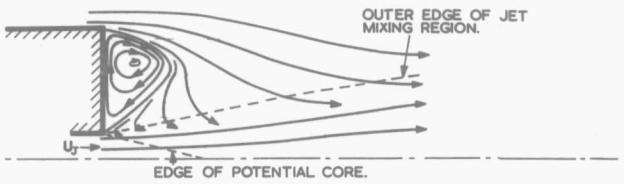

FIG. 6c. JET VELOCITY SONIC OR DESIGN.

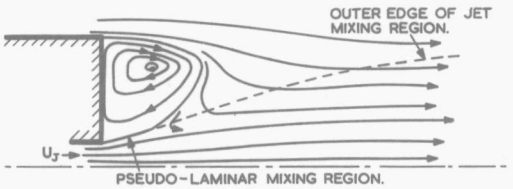

FIG. 6d. JET VELOCITY SLIGHTLY GREATER THAN DESIGN.

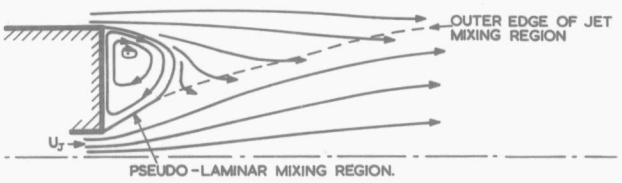

FIG. 6e. JET MUCH UNDER-EXPANDED AT EXIT.

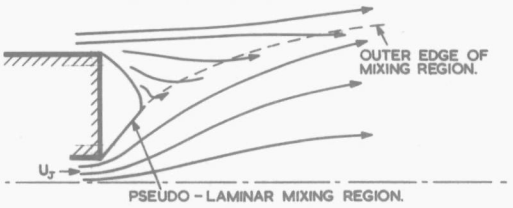

FIG. 6f. COMPRESSIVE EFFECT OF SEVERELY UNDER-EXPANDED JET.

FIG. 6. FLOW IN MIXING REGION. [DIAGRAMMATIC.]

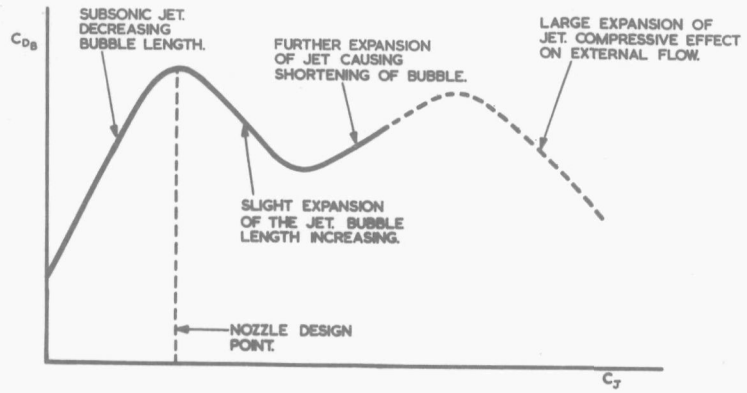

FIG. 7 EFFECT OF VARIATIONS IN FLOW CHARACTERISTICS ON THE BASE DRAG.

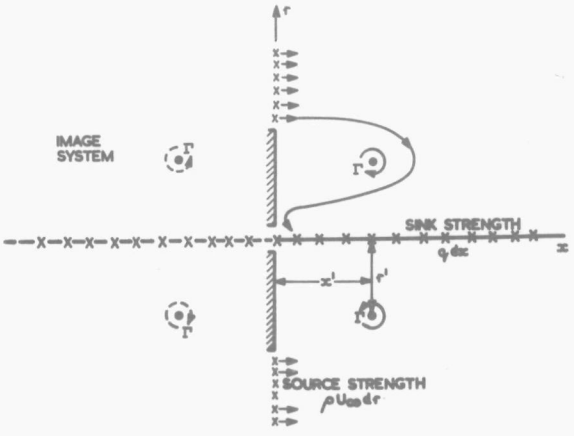

FIG. 8. POTENTIAL FLOW MODEL FOR BASE REGION.

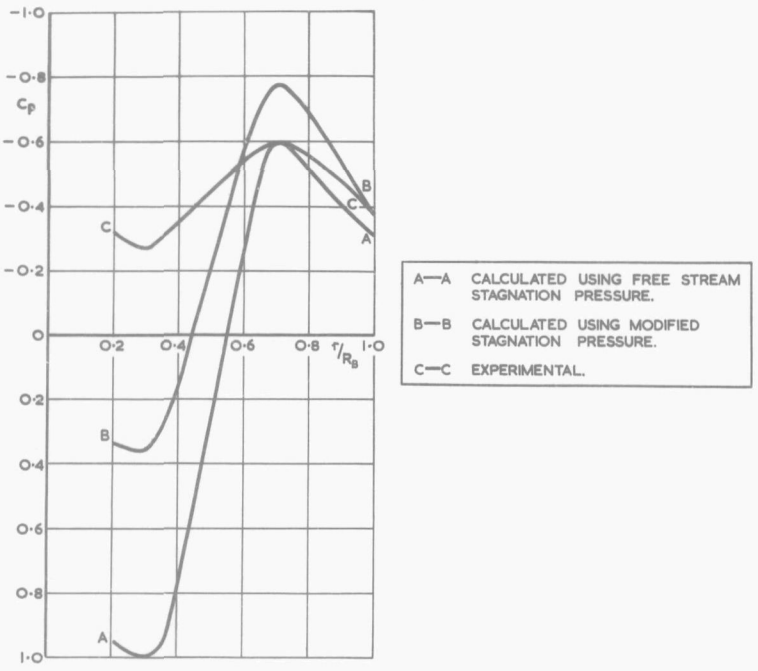

FIG. 9. COMPARISON BETWEEN POTENTIAL FLOW MODEL AND EXPERIMENT.

SUBSONIC JET $U_J/U_\infty = 6$

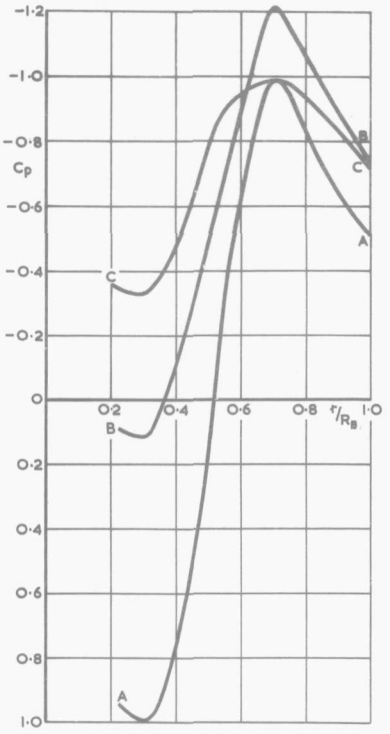

FIG. 10 COMPARISON BETWEEN POTENTIAL FLOW MODEL AND EXPERIMENT.

SONIC JET $U_J/U_\infty = 10$

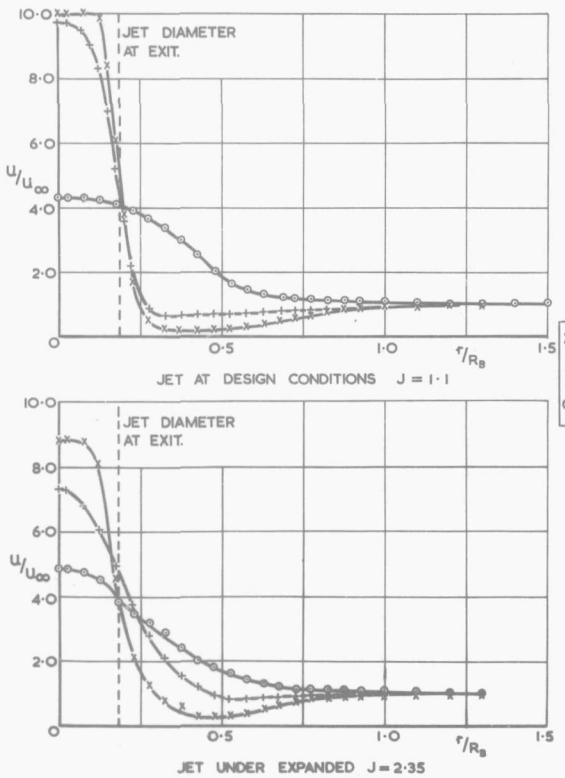

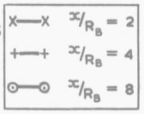

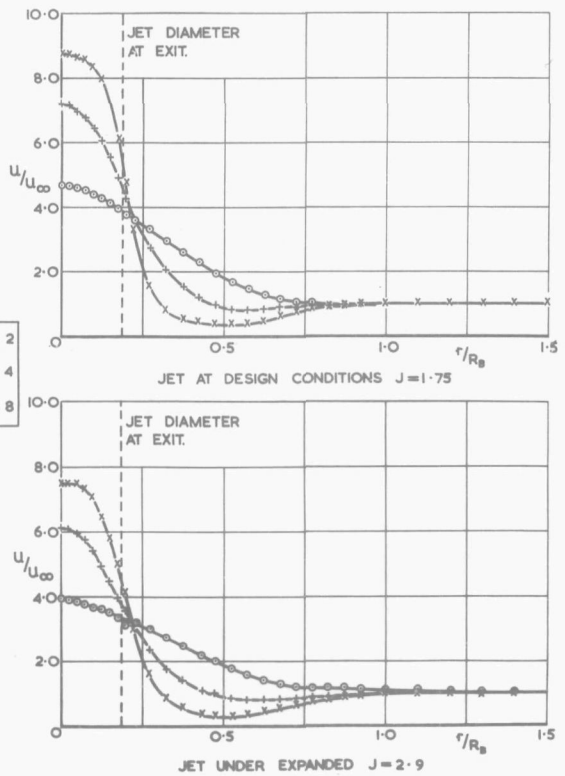

FIG. 11. TYPICAL VELOCITY PROFILES. SONIC JET.

FIG. 12 TYPICAL VELOCITY PROFILES. JET DESIGN MACH NUMBER = 1·98